THE JOURNAL OF PHYSICAL CHEMISTRY B

ARTICLE

pubs.acs.org/JPCB

Impact of Nanoclay on Isothermal Cold Crystallization Kinetics and Polymorphism of Poly(L-Lactic Acid) Nanocomposites

Nadarajah Vasanthan,*[,†] Hoang Ly,[†] and Subhas Ghosh[‡]

[†]Department of Chemistry, Long Island University, One University Plaza, Brooklyn, New York 11201, United States

[‡]College of Technology, Eastern Michigan University, 10 Roosevelt Hall, Ypsilanti, Michigan 48197, United States

ABSTRACT: Poly(L-lactic acid) (PLLA) intercalated nanocomposite films containing 1, 2, 5, and 10% organically modified montmorillonite (OMMT) have been synthesized by the solvent casting approach. The thermal characteristics, isothermal cold crystallization kinetics, and structural changes of neat PLLA and its nanocomposites during annealing were studied by using differential scanning calorimetry (DSC) and Fourier transform infrared (FTIR) spectroscopy. DSC observation showed that melting temperature and final crystallinity were not affected significantly with OMMT loading. PLLA films with increasing OMMT content exhibited higher crystallization rates than neat PLLA during annealing and suggested that the silicate platelets act as a nucleation agent during annealing. The effect of OMMT content on the isothermal crystallization kinetics of PLLA was analyzed using the Avrami equation. An Avrami constant of 1−2 was observed, suggesting that crystallization proceeds through one-dimensional growth with heterogeneous nucleation. FTIR investigation showed a band at 922 cm^{-1} at all T_a, and no band at 908 cm^{-1} suggested that all samples form α crystal regardless of OMMT content or T_a.

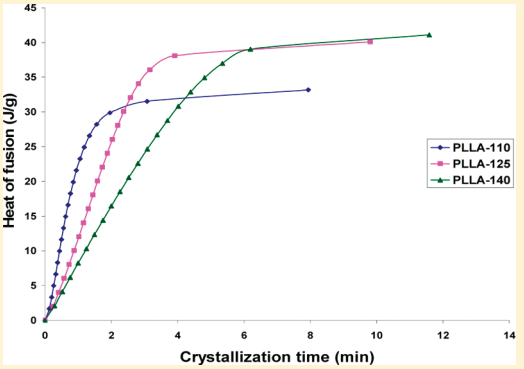

1. INTRODUCTION

Poly(lactic acid) (PLA) is a biodegradable aliphatic polyester, and it is used for a range of biomedical applications such as drug delivery devices, scafold fabrication, and tissue regeneration.[1−10] PLA is produced from renewable resources such as corn, sugar cane, and sugar beets.[11,13] It is of great interest to produce high-strength fibers and films for commercial applications from poly-(L-lactic acid) (PLLA), which is a biodegradable product.[14−20] Solution spinning,[17,18,20] melt spinning/hot drawing,[14,16,19] and high-speed melt spinning[15] methods have been applied to the PLLA fibers to improve the mechanical properties. The highest tensile modulus (16 GPa) and strength (2.1 GPa) has been achieved by Pennings et al. with dry spinning/hot drawing methods. These mechanical properties, however, resulted only from high molecular weight polymers ($M_v > 10^5$).[18,19]

Polymer nanocomposites have received considerable attention in recent years, because they often produce superior mechanical and physical properties such as high strength, high stiffness, and higher heat resistance compared to micro- and macrocomposites.[21−29] In general, the addition of clay nanoparticles impacts polymer crystallization. It has been shown that crystallization and crystallization kinetics can be altered by introducing nanoparticles in the polymer matrix. Intercalated and exfoliated PLLA nanocomposites were prepared, and melt crystallization studies were conducted by crystallizing from the melt slowly.[24−29] It has been demonstrated that the rate of crystallization increased for intercalated composites and somewhat retarded in the exfoliated composites.[28] If the amorphous polymers are heated above its T_g, crystallization occurs, and this phenomenon is called cold crystallization.[30−34] To our knowledge, no studies have been conducted on isothermal cold crystallization of PLLA nanocomposites. In the present study, we prepared a series of PLLA intercalated nanocomposites and studied the isothermal cold crystallization and crystallization kinetics using Fourier transform infrared (FTIR) spectroscopy and differential scanning calorimetry (DSC). The principle aim of this work is to understand the effect of clay content on isothermal cold crystallization kinetics and polymorphism of PLLA intercalated nanocomposites and compare with isothermal melt crystallization.

2. EXPERIMENTAL SECTION

2.1. Materials. PLLA with molecular weight of 325 000 g/mol was purchased from Polysciences, Inc. Montmorillonite K10 (MMT-K10), dichloromethane (ACS spectrophotometric grade), and dodecylamine were purchased from Sigma-Aldrich. The concentrated hydrochloric acid was obtained from Fisher Scientific (ACS grade). All of these materials were used without further purification.

2.2. Preparation of Organophilic Clay (Organically Modified Montmorillonite) (OMMT). Organophillic clay was prepared using a method reported in the literature.[21] Dodecylamine (8.82 g) was placed in a 500 mL beaker with 4.8 mL of

Received: April 9, 2011
Revised: June 28, 2011
Published: June 30, 2011

concentrated hydrochloric acid and 100 mL of water. The above solution was heated and stirred at 80 °C. At the same time, 20 g of MMT-K10 and 400 mL of water were placed in a 800 L beaker, and the dispersion was also heated and stirred at 80 °C. The dodecylamine solution was poured into the MMT dispersion, and the mixture was stirred vigorously for an hour at 80 °C. A white precipitate was formed and collected by vacuum filtration. The white precipitate was then placed in a 600 mL beaker with 400 mL of hot water and stirred continuously for about 1 h. This procedure was repeated twice in order to remove all of the ammonium salt of dececylamine. Finally, the organophilic clay or modified-MMT was collected by vacuum filtration and dried at room temperature.

2.3. Preparation of Neat PLLA and PLLA-OMMT Films. PLLA films with various percentages of OMMT by weight such as PLLA containing 0, 1, 2, 5, and 10% OMMT were prepared by the solvent casting technique as described below. Neat PLLA and PLLA containing 1, 2, 5, and 10% OMMT were labeled as PLLA, PLLA1, PLLA2, PLLA5 and PLLA10, respectively. PLLA pellets (250 mg) and an appropriate amount of OMMT was dissolved in 25 mL of dichloromethane. Half of the dichloromethane was used to dissolve the PLLA pellets, and the other half of the dichloromethane was used to disperse the OMMT. Both the PLLA solution and the OMMT dispersion were heated and stirred separately at about 40 °C. When all PLLA pellets were dissolved completely, the OMMT dispersion was poured into the PLLA solution. The mixture was heated and stirred until it was dispersed uniformly in the PLLA solution. The PLLA−OMMT mixture (5.0 mL) was poured on a glass plate. The thin film was peeled off and dried for several days at room temperature.

2.4. Wide-Angle X-ray Diffraction (WAXD). WAXD of neat PLLA, PLLA nanocomposites, and OMMT was performed using a SCINTAG XGEN-400 at room temperature. The CuKα radiation of 1.54 Å wavelegnth was operated at 40 kV and 40 mA. The diffracting intensities were recorded in 0.02° 2θ steps over the range of $2° < 2\theta < 40°$. All experiments were performed in the reflection mode. The d spacing of the MMT was determined from the peak position $d_{(001)}$ reflection in the WAXD diffractograms using the Bragg equation.

2.5. Differential Scanning Calorimetry. DSC experiments were performed with a Perkin-Elmer DSC 7. The instrument was calibrated for temperature and heat of fusion using standard indium (T_m = 156.6 °C and ΔH = 28.5 J/g). All experiments were performed under nitrogen atmosphere with a flow rate of 20 mL/min. 4−6 mg samples were used for all measurements. Crystallinity of neat PLLA and PLLA nanocomposite samples were obtained using heating scan. Onset temperatures were taken as transition temperatures. A baseline under the peak was drawn by connecting the flat baseline before and after the peak. The integrated peak area under the peak was taken as the heat of fusion. The crystallinity of PLLA was calculated by using the following equation:

$$X_c = \Delta H_s/\Delta H_o$$

where ΔH_s is the heat of fusion of the sample crystallization. ΔH_o was taken as 93.0 J/g.[35]

Crystallization kinetics study of neat PLLA and PLLA nanocomposites were performed by annealing directly inside the DSC at annealing at temperatures of 110 °C, 125 °C, and 140 °C. After the sample was held for 5 min at 25 °C and it was heated from 25 °C to the desired annealing temperature at a heating rate of 100 °C/min. Crystallization was followed for 30 min using crystallization exotherm. After the crystallization was completed, the samples was reheated to 200 at 10 °C/min.

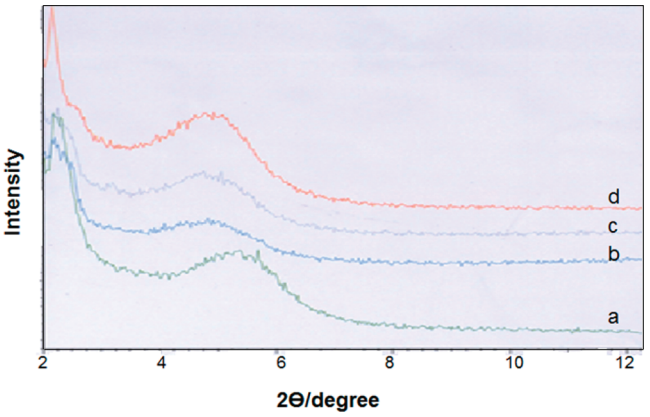

Figure 1. WAXD patterns of OMMT and PLLA nanocomposites with varying OMMT content: (a) OMMT (b) PLLA with 2 wt % OMMT, (c) PLLA with 5 wt % OMMT, and (d) PLLA with 10 wt % OMMT.

2.6. FTIR Spectroscopy. Infrared spectra of the annealed and hydrolyzed PLLA films were collected using a Nicolet Magna 760 spectrometer with MCT detector using transmission mode. The spectra were collected with a resolution of 4 cm^{-1} and 64 scans per sample in the mid-IR region of 4000 to 500 cm^{-1}. Grams software was used for peak fitting. The linear baseline and Lorentzian shape were used for all peak fitting curves.

3. RESULTS AND DISCUSSION

3.1. Thermal Characteristics. PLLA nanocomposites with 1, 2, 5, and 10% OMMT nanocomposites were prepared to examine the influence of nanoclay on cold crystallization and crystallization kinetics. The evidence for intercalated or exfoliated nanocomposite is usually obtained either by WAXD or transmission electron microscopy (TEM) or both.[36−39] The WAXD pattern of PLLA nannocomposites along with neat PLLA and OMMT is shown in Figure 1. The OMMT and nanocomposites shows characteristic reflections at 5.55 and 4.75°, respectively. These reflections correspond to d-spacing (d_{001}) of 1.50 and 1.70 nm, respectively. It can also be seen that the intensity of the reflection increases with increasing OMMT content. The increase in d-spacing with OMMT in the PLLA matrix suggests that these nanocomposites are predominantly intercalated.

All PLLA nanocomposite films were prepared at room temperature and annealed at 80−140 °C. DSC scans of neat PLLA and PLLA nanocomposite with 1 wt % OMMT (PLLA1) at different T_a are shown in Figure 2. It should be noted that the neat PLLA sample not annealed shows two transitions, cold crystallization exotherm (T_{cc}) and melting endotherm (T_m), while neat PLLA annealed at temperatures from 80° to 140 °C shows only melting endotherm (T_m). The melting peak, T_m, is shifted to higher temperatures as annealing temperature (T_a) increases. The difference in T_m between neat PLLA not annealed and PLLA annealed at 140 °C is about 10 °C. Similar observation was made for PLLA nanocomposites with various amount of OMMT. A DSC scan of PLLA1 nanocomposite at room temperature also shows two transitions, T_{cc} and T_m, while the DSC curves of annealed PLLA nanocomposites show only single transition, T_m. T_m shows an increase with increasing T_a for all PLLA nanocomposites.

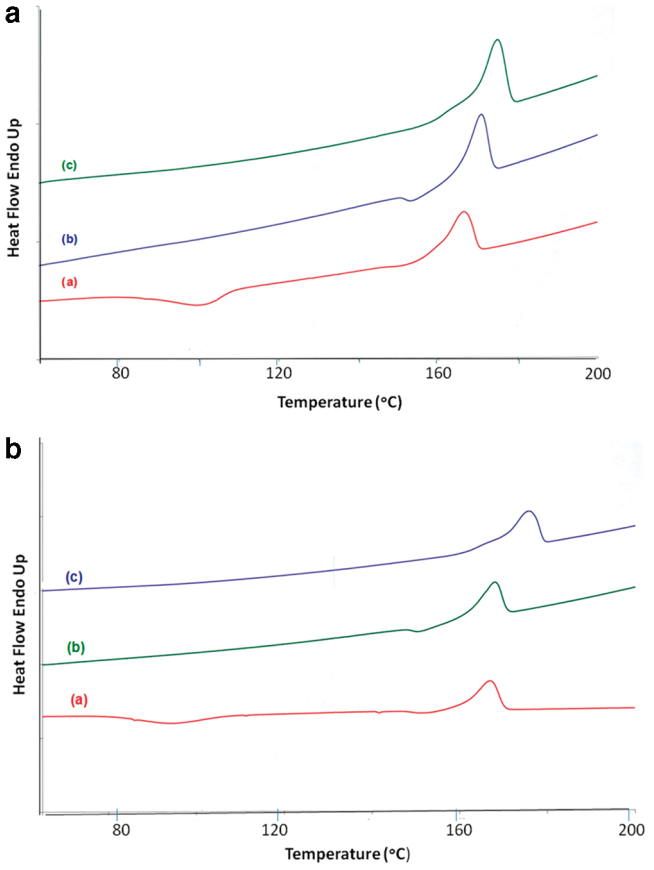

Figure 2. (a) DSC curves of neat PLLA at various annealing temperatures: (a) neat PLLA at room temperature, (b) neat PLLA annealed at 80 °C, and (c) neat PLLA annealed at 140 °C. (b) DSC curves of PLLA naocomposite with 1 wt % OMMT at various annealing temperatures: (a) as cast, (b) annealed at 80 °C, and (c) annealed at 140 °C.

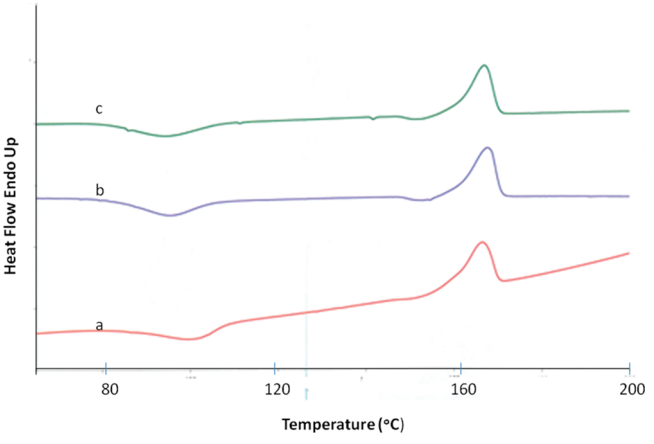

Figure 3. DSC scans of neat PLLA and its nanocomposites at room temperature: (a) neat PLLA, (b) PLLA with 5 wt % OMMT, and (c) PLLA with 10 wt % OMMT.

DSC scans of PLLA nanocomposite samples with different amounts of OMMT compositions are shown in Figure 3 along with DSC scan of neat PLLA. Both transitions, T_{cc} and T_m, are apparent in all DSC scans. T_{cc} occurs in the region between 80 and 90 °C, and it is slightly shifted to lower temperature with the addition of OMMT as compared to neat PLLA. For example, T_{cc} shifts from 85 to 83 °C when OMMT composition increased from 0−10 wt % in PLLA. It can be seen that the T_{cc} of PLLA nanocomposite is broader than that of neat PLLA. No significant change was observed in T_m with the addition of OMMT in PLLA. The T_m of neat PLLA and its nanocomposites were plotted against T_a in Figure 4. It is clear from Figure 4 that the samples annealed at the same T_a have no significant change in T_m, indicating that OMMT loading does not alter the melting temperature of PLLA. This observation suggests that the lamella thickness of the crystals does not change with increasing OMMT compositions in PLLA at the same T_a. However, T_m increases by 10−11 °C when T_a increases from room temperature to 140 °C, implying that the lamella thickness of the PLLA crystals formed during annealing strongly depends on T_a but not with the amount of OMMT.

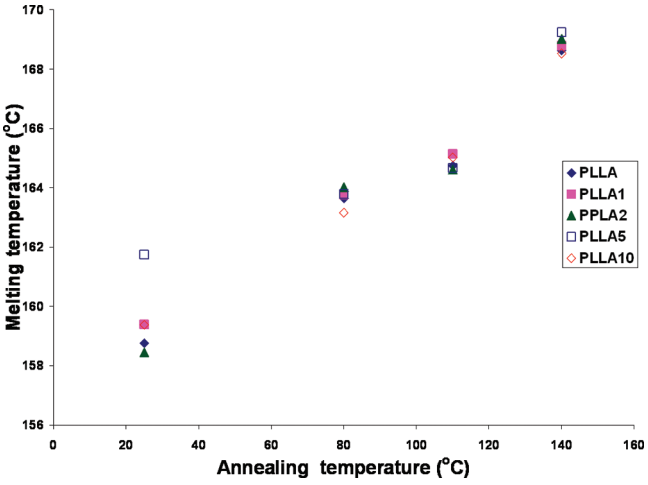

Figure 4. Melting temperature versus annealing temperature for neat PLLA and its nanocomposites.

Heat of fusion was determined by integrating the area under the melting peak of the DSC curves, and it is directly proportional to the degree of crystallinity. The degree of crystallinity, χ_c, is determined using the following equation:

$$\chi_c = \frac{\Delta H_f}{(1-\phi)\Delta H^*} \times 100\% \quad (1)$$

Where ΔH_f is heat of fusion for the PLLA sample, ΔH^* is the heat of fusion for PLLA with 100% crystallinity (93 J/g), and ϕ is the weight fraction of OMMT in the PLLA sample.[35]

Figure 5 shows the degree of crystallinity of PLLA annealed at various T_a as a function of OMMT content. No significant change in crystallinity was observed for PLLA samples annealed at higher T_a with OMMT content. However, increasing T_a, independent of OMMT composition in PLLA nanocomposites, increases the crystallinity, indicating that the crystallinity mainly depends on T_a, and OMMT loading has no significant effect on final crystallinity. Crystallinity changes have been studied with increasing OMMT content for various intercalated and exfoliated PLLA nanocomposites during melt crystallization. It has been shown that crystallinity decreases with increasing OMMT content for exfoliated nanocomposites, whereas crystallinity decreases slightly with increasing OMMT content for intercalated nanocomposite.[27−29]

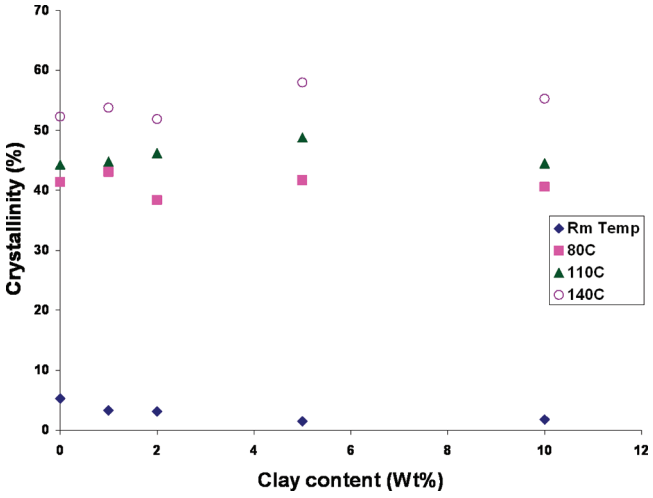

Figure 5. Crystallinity of neat PLLA and its nanocomposites annealed at various temperatures.

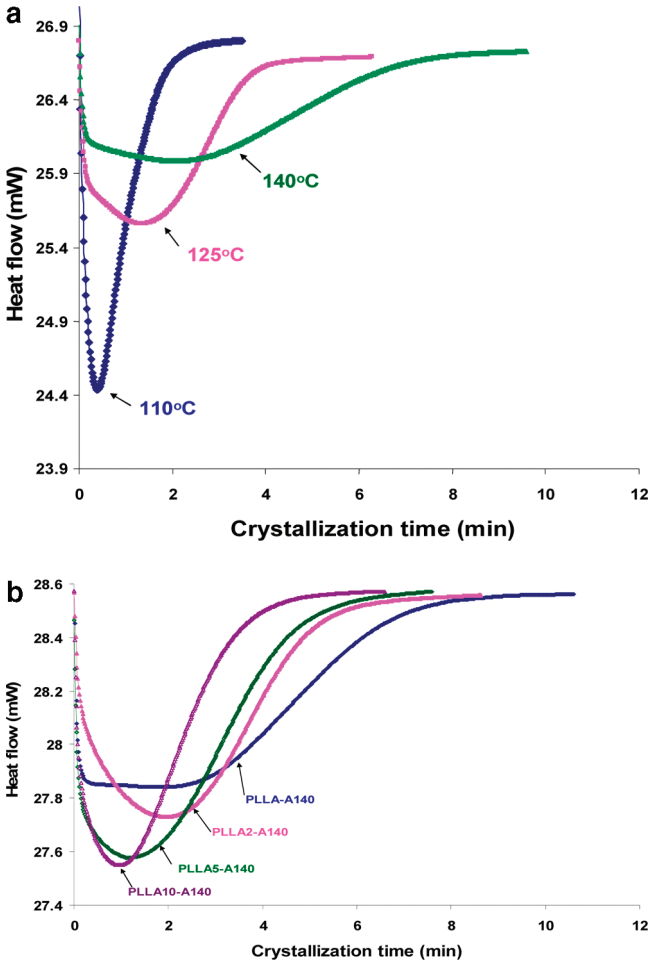

Figure 6. (a) Crystallization exotherms crystallization of neat PLLA annealed from 110 to 140 °C. (b) Crystallization exotherms of PLLA nanocomposites with various OMMT contents annealed at 140 °C.

3.2. Isothermal Cold Crystallization Kinetics. Isothermal cold crystallization kinetics of PLLA and its nanocomposites was performed by annealing the sample directly inside the DSC at 110, 125, and 140 °C. The development of crystallization was followed using crystallization exotherms. DSC curves of neat PLLA samples crystallized at T_a from 110 to 140 °C are shown in Figure 6a. The rate of crystallization decreases with increasing T_a, suggesting a nucleation-controlled regime.[40] DSC curves of PLLA nanocomposites with various amounts of OMMT crystallized at 140 °C are depicted in Figure 6b. It shows that the crystallization exotherm gets more distinct with increasing OMMT loading in PLLA, indicating that OMMT enhances the rate of crystallization of PLLA by improving crystalline order. Similar DSC curves were obtained for PLLA nanocomposites crystallized at other T_a. A strong interaction between OMMT platelets and polymer chain increases the crystallization rate.

The crystallization time, t, is the time required to complete the crystallization process. Crystallization time (t) can be obtained from the crystallization exotherm versus time plot when there is no change in the crystallization exotherm. It appears that t increases with increasing T_a, while t decreases with the increasing OMMT loading. Isothermal crystallization kinetics of PLLA and its nanocomposite samples annealed at various T_a were analyzed using the Avrami equation.[41,42] Relative crystallinity development is directly proportional to the evolution of heat released during the crystallization process. This relationship is depicted as

$$\chi_t = \frac{\int_0^t (dH/dt)\, dt}{\int_0^\infty (dH/dt)\, dt} \quad (2)$$

where the numerator represents the heat generated at time t, while the denominator represents the total heat that was generated for the entire crystallization process. Using eq 2, the fraction of the relative crystalline phase, χ_t, for the sample at a particular time t was calculated. Figure 7a,b shows the heat of fusion as a function of crystallization time for neat PLLA and its nanocomposite containing 2% OMMT at various T_a. Similar plots were also obtained for other PLLA nanocomposites crystallized at temperatures from 110 to 140 °C.

Isothermal crystallization kinetics of neat PLLA and PLLA nanocomposites can be described by using the classical Avrami equation as follows:

$$1 - \chi_t = \exp(-kt^n) \quad (3)$$

where χ_t is crystalline fraction at a particular time t, n is the Avrami exponent that is normally an integer between 1 and 4, k is an Avrami parameter, and t is the crystallization time. Taking double natural logarithms of eq 3 leads to:

$$\ln[-\ln(1-\chi_t)] = n \ln t + \ln k \quad (4)$$

The Avrami exponent, n, was obtained from the plot of $\ln[-\ln(1-\chi_t)]$ versus $\ln t$. The plots of $\ln[-\ln(1-\chi_t)]$ versus $\ln t$ are shown in Figure 8 for neat PLLA samples crystallized at different T_a from 110 to 140 °C. The plots for PLLA nanocomposites crystallized at various T_a were similarly obtained. Only the experimental data between 5 and 70% relative crystallinity were used for the calculation of the Arvami exponent, n, because the data above 70% crystallinity may deviate from linearity.

Crystallization kinetics data of neat PLLA and its nanocomposites were obtained from the Avrami plot, and they are summarized in Table 1. Linear regression of these straight lines provided the Avrami exponent (n) and the rate constant (k). The values for n depend on the crystallization mechanism, and n

dx.doi.org/10.1021/jp203322d |J. Phys. Chem. B 2011, 115, 9556–9563

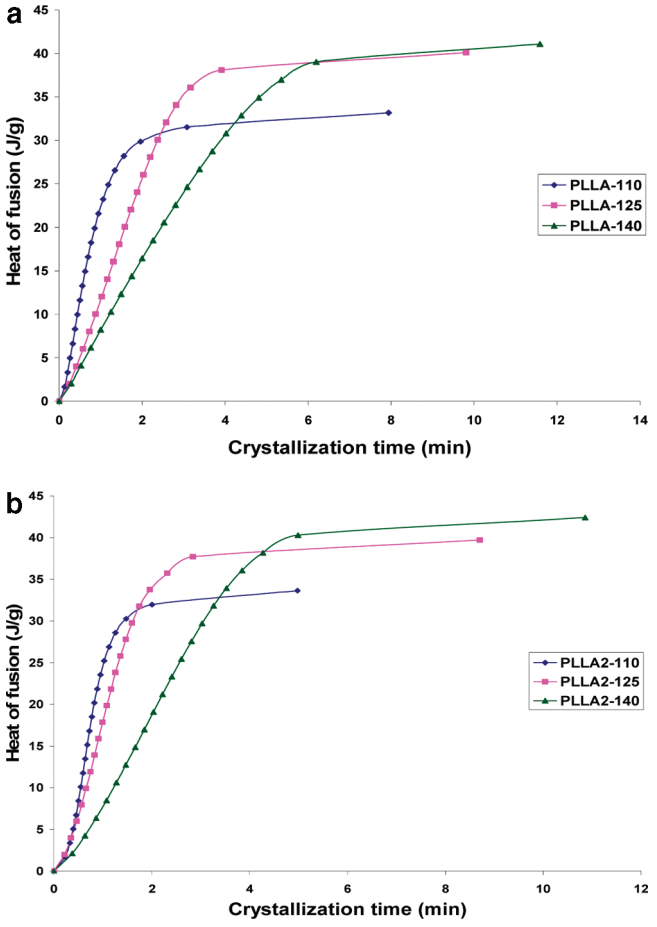

Figure 7. (a) Heat of fusion with respect to crystallization time for neat PLLA at various annealing temperatures. (b) Heat of fusion with respect to crystallization time for PLLA nanocomposite containing 2 wt % OMMT at various annealing temperatures.

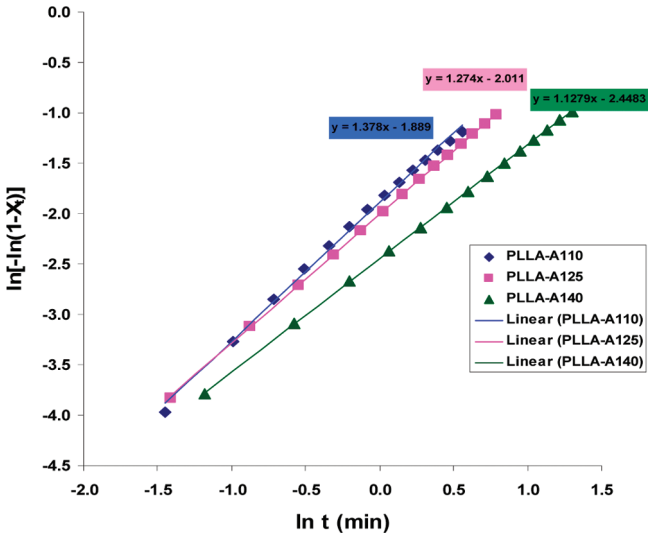

Figure 8. Avrami plots of $\ln[-\ln(1-\chi_t)]$ versus $\ln t$ for the neat PLLA annealed at various temperatures.

usually takes an integer number between 1 and 4. It was reported for various polymers that the n value adopts fractional numbers

Table 1. The Results from the Isothermal Crystallization Kinetic Study for Neat PLLA and Its Nanocomposites

OMMT content (wt %)	T_a (°C)	$t_{1/2}$ (min)	n
0	110	1.351	1.4
0	125	1.589	1.3
0	140	2.576	1.1
2	110	1.331	1. 6
2	125	1.381	1.5
2	140	2.223	1.4
5	110	1.129	1.6
5	125	1.204	1.4
5	140	1.820	1.2
10	110	0.891	1.6
10	125	1.097	1.5
10	140	1.353	1.3

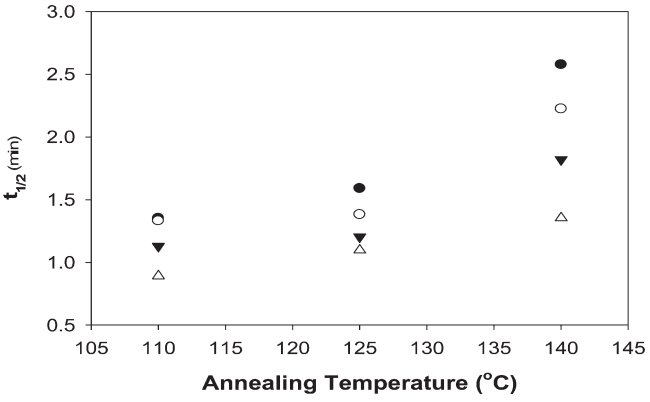

Figure 9. Crystallization half-time as a function of annealing temperature for neat PLLA and PLLA nanocomposites.

due to secondary crystallization. The values of n were found between 1.1 and 1.6, depending on the temperature. This result also shows that OMMT content has no significant effect on n values. The lower n value indicates that crystal growth proceeds in one dimension. The value of n observed in this study is smaller than the value reported by Zhang et al. for cold crystallization.[43,44] The smaller n value may be attributed to a faster crystallization mechanism that does not provide enough time to grow in three dimensions.

The crystallization half time $t_{1/2}$ is one of the most interesting characteristics of crystallization kinetics studies. The $t_{1/2}$ is defined as the time at which 50% of the relative crystallinity is developed. The values of $t_{1/2}$ for neat PLLA and PLLA nanocomposites were obtained from DSC scans and are also summarized in Table 1. The $t_{1/2}$ values are plotted as a function of T_a in Figure 9. The $t_{1/2}$ increased with increasing T_a. Figure 9 shows a clear evidence for a given annealing temperature in which neat PLLA has a higher value of $t_{1/2}$ than PLLA nanocomposites, indicating that neat PLLA has a slower crystallization rate than its nanocomposites. It appears that more nucleation sites are available with increasing OMMT content. Therefore it can be concluded that OMMT acts as a nucleating agent for PLLA crystallization and favors the heterogeneous nucleation.

3.3. FTIR Spectroscopy. In the present study, FTIR spectroscopy is used to investigate the structural changes of neat PLLA

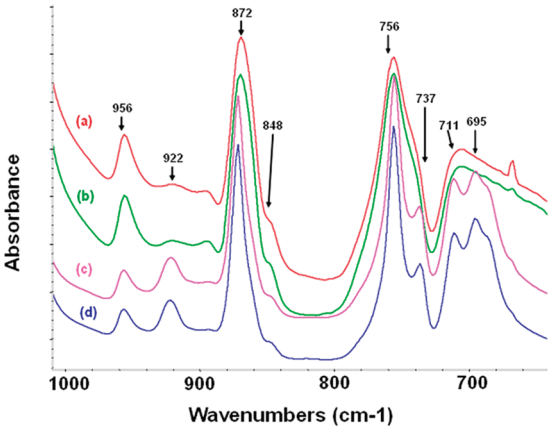

Figure 10. The IR spectra of neat PLLA samples annealed at various temperatures in the region 1000−650 cm^{-1}: (a) neat PLLA at room temperature, (b) neat PLLA annealed at 80 °C, (c) neat PLLA annealed at 110 °C, and (d) neat PLLA annealed at 140 °C.

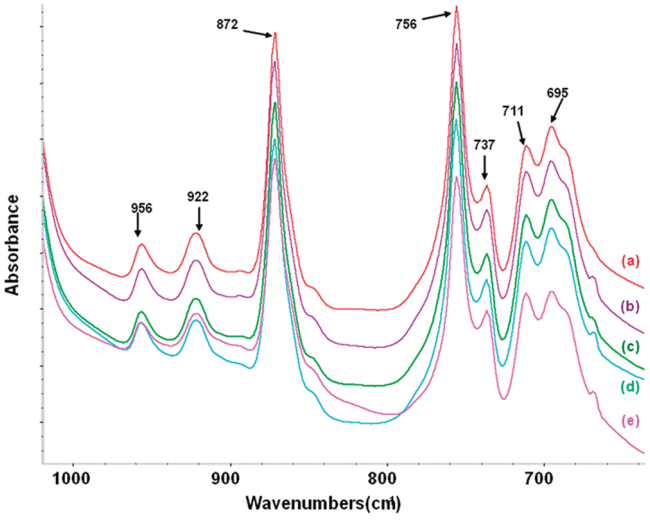

Figure 11. The IR spectra of neat PLLA and its nanocomposites annealed at 140 °C in the region 1000−650 cm^{-1}: (a) neat PLLA, (b) PLLA nanocomposite with 1 wt % OMMT, (c) PLLA nanocomposite with 2 wt % OMMT, (d) PLLA nanocomposite with 5 wt % OMMT, and (e) PLLA nanocomposite with 10 wt % OMMT.

and its nanocomposites during annealing. It was reported previously that the IR spectra in the regions 1000−650 cm^{-1} and 1500−1250 cm^{-1} are very sensitive to the structural changes taking place during the crystallization.[29,43−45] Figure 10 shows the FTIR spectra of neat PLLA in the region 1000−650 cm^{-1} with increasing T_a. It was observed that the bands at 922, 872, 756, and 695 cm^{-1} increase in absorbance, and the bands at 956, 848, 737, and 711 cm^{-1} decrease in absorbance as T_a increases. The effect of OMMT content on the IR spectra of PLLA nanocomposites was also studied using FTIR spectroscopy. The IR spectra of neat PLLA and its nanocomposites annealed at 140 °C in the region from 1000 to 650 cm^{-1} are shown in Figure 11 with varying OMMT loading. No significant change was observed in the regions from 1000 to 650 cm^{-1} with OMMT loading at the same T_a. Similar IR spectra were obtained for neat PLLA and its nanocomposites annealed at 80 and 110 °C,

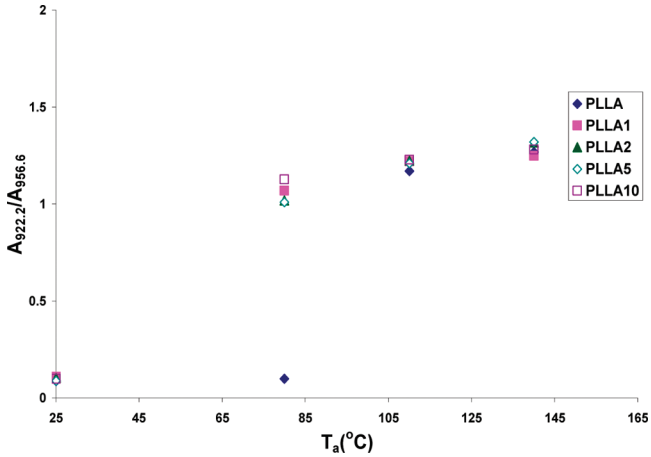

Figure 12. Band ratio of 922 cm^{-1}/ 956 cm^{-1} as a function of annealing temperatures for neat PLLA and its nanocomposites.

suggesting that the presence of OMMT in PLLA has no significant effect on chain conformation of PLLA.

In general, PLLA crystallizes into three possible crystal forms: α, β, and γ crystal forms. The most common α crystal form is obtained either by melt or solution crystallization, while the β crystal form is obtained during drawing at high draw ratios and temperatures. The γ form was obtained during epitaxial crystallization. It has been shown that the α form of PLLA from solution-spun fibers has a pseudo-orthorhombic unit cell containing two left-handed 10_3 polymeric helices arranged in an antiparallel fashion.[46−48] The unit cell dimensions of the α crystal form are a = 1.07 nm, b = 0.645 nm, and c = 2.78 nm. Hoogsteen[49] et al. showed that the β form of PLLA adopts an orthorhombic unit cell containing six left-handed 3_1 polymeric helices. The unit cell dimensions of β form are a = 1.031 nm, b = 1.821 nm, and c = 0.900 nm. Infrared band assignments were reported, and it was shown that the band at 922 cm^{-1} is associated with α crystalline phase, while the band at 908 cm^{-1} is associated with the β crystalline phase. The band at 956 cm^{-1} is associated with the amorphous phase. These bands were assigned to the coupling of C−C backbone stretching with the CH_3 rocking mode, which is very sensitive to the 10_3 helical chain conformation of the α-crystals. Figure 10 shows no band at 908 cm^{-1}, suggesting that there is no detectable level of β crystal form present in our annealed PLLA. A similar observation was made for PLLA nanocomposites containing various amounts of OMMT.

PLLA films annealed over the range of temperature from 80 to 130 °C has been studied recently by FTIR spectroscopy.[50] A method has been developed to obtain the crystallinity of PLLA. A very good correlation between the band ratios between 922 and 956 cm^{-1} and DSC crystallinity was observed. The band ratios of 922 and 956 cm^{-1} of PLLA and its nanocomposites were plotted against T_a in Figure 12. It is apparent from Figure 11a that the band ratio increases with increasing T_a independent of OMMT composition in PLLA. This is in good agreement with our DSC results, which show no effect on crystallinity with increasing OMMT content. The band ratio of 922 cm^{-1}/956 cm^{-1} as a function of crystallinity obtained by DSC of PLLA and its nanocomposites is plotted in Figure 13. It can be seen that the band ratio increases as crystallinity increases, and a very good correlation was observed. This further confirms that the band

dx.doi.org/10.1021/jp203322d |J. Phys. Chem. B 2011, 115, 9556–9563

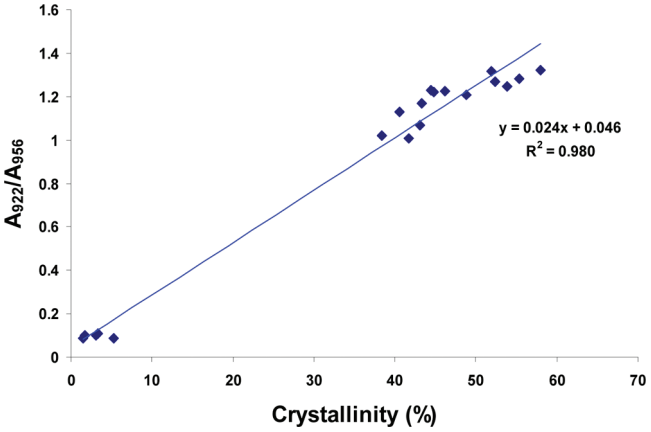

Figure 13. The plot of band ratio at 922 cm^{-1} over 956 cm^{-1} as a function of crystallinity of neat PLLA and its nanocomposites at various T_a.

ratio of 922 cm^{-1}/956 cm^{-1} can be used to measure the crystallinity of PLLA nanocomposites.

4. CONCLUSIONS

Thermally induced crystallization and crystallization kinetics of neat PLLA and its nanocomposites with OMMT were investigated. PLLA and its nanocomposite films showed both T_m and T_{cc}, while that annealed at T_a from 80 to 140 °C showed only T_m. T_{cc} was found to decrease slightly from 85 to 83 °C with OMMT loading, whereas T_m increased by 10 °C as T_a increased from room temperature to 140 °C. The final crystallinity increased with annealing temperatures regardless of OMMT loading, and OMMT content showed no effect on final crystallinity. The rate of crystallization was found to depend on OMMT content and crystallization temperature. The Avrami exponent, n, was found to be between 1 and 2, suggesting one-dimensional growth. The crystallization half time $t_{1/2}$ of PLLA nanocomposites was found to be lower than $t_{1/2}$ of neat PLLA, indicating that the rate of crystallization increases with increasing OMMT content in the PLLA matrix. FTIR investigation showed a band at 922 cm^{-1} at all T_a and no band at 908 cm^{-1}, suggesting that all samples form α crystal regardless of OMMT content or T_a. The ratio of the band at 922 cm^{-1} and the band at 956 cm^{-1} increased as the function of T_a regardless of OMMT content in PLLA. A very good correlation was observed between the band ratios and DSC crystallinity.

■ ACKNOWLEDGMENT

This study was supported by the National Textile Center and Long Island University. The authors are also indebted to Oanh Ly for performing IR measurements and Astrid Campo for the X-ray measurements.

■ REFERENCES

(1) Nostrum, C. V.; Veldhuis, F. J.; Bos, G. W.; Hennink, W. E. *Polymer* **2004**, *45*, 6779.
(2) Reeve, M. S.; McCarthy, S. P.; Downey, M. J.; Gross, R. A. *Macromolecules* **1994**, *27*, 825.
(3) Park, J. H.; Jana, S. C. *Polymer* **2002**, *42*, 8759–68.
(4) Wu, C. L.; Zhang, M. Q.; Rong, M. Z.; Friedrich, K. *Compos. Sci. Technol.* **2002**, *62*, 1327–40.
(5) Fleming, R. G.; Murphy, C. J.; Abrams, G. A.; Goodman, S. L. *Biomaterials* **1999**, *20*, 573–588.
(6) Lee, J. H.; Park, T. G.; Park, H. S.; Lee, D. S.; Lee, Y. K.; Yoon, S. C.; Nam, J. D. *Biomaterials* **2003**, *24*, 2773–2778.
(7) Langer, R.; Vacanti, J. P. *Science* **2002**, *260*, 920–926.
(8) Khang, G.; Lee, S. J.; Jeon, J. H.; Lee, H. B. *Polymer* **1999**, *24*, 869–876.
(9) Meredith, J. C.; Sormona, J. L.; Keselowsky, B. G.; Tona, A.; Karim, A.; Amis, E. J. *J. Biomed. Mater. Res.* **2003**, *66*, 483–490.
(10) Li, S.; Vert, M. Biodegradable aliphatic polyesters. In *Degradable Polymers: Principle and Applications*; Scott, G., Gilead, D., Eds.; Chapman & Hall: London, 1995.
(11) Ikada, Y; Tsuji, H. *Macromol. Rapid Commun.* **2000**, *21*, 117–132.
(12) Urayama, H.; Kanamori, T.; Fukushima, K.; Kimura, Y. *Polymer* **2003**, *44*, 5635.
(13) Lunt, J.; Shafer, A. L. *J. Ind. Text.* **2000**, *29*, 191–205.
(14) Okuzaki, H.; Kubota, I.; Kunugi, T. *J. Polym. Sci., Part B: Polym. Phys.* **1999**, *37*, 991.
(15) Mezghani, K; Spruiell, J. E. *J. Appl. Polym. Sci.* **1997**, *36*, 1005–1012.
(16) Kulkarni, R. K.; Moore, E. G.; Hegyeli, A. F.; Lenord, F. *J. Biomed. Mater. Res.* **1971**, *5*, 169.
(17) Hyon, S. H.; Jamshidi, K.; Ikada, Y. In *Polymers as Biomaterials*; Shalby, S. W., Ed.; Plenum Press: New York, 1984.
(18) Eling, B.; Gogolewski, S.; Penning, A. J. *Polymer* **1982**, *23*, 1587–1593.
(19) Leenslag, J. W.; Penning, A. J. *Polymer* **1987**, *28*, 1695.
(20) Tsui, H.; Ikada, Y.; Hyon, S. H.; Kimura, Y.; Kaito, T. J. *J. Appl. Polym. Sci.* **1994**, *51*, 337.
(21) Kojima, Y.; Usuki, A.; Kawasumi, M.; Okada, A.; Kurachi, T; Kamigaito, O. *J. Polym. Sci., Part A: Polym. Chem.* **1993**, *31*, 983–986.
(22) Messersmith, P. B.; Ginnelis, E. P. *J. Polym. Sci., Part A: Polym. Chem.* **1995**, *33*, 1047–1057.
(23) Liu, X.; Wu, Q.; Zhang, Q; Mo, Z. *J. Polym. Sci., Part B: Polym. Phys.* **2003**, *41*, 63.
(24) Sinha Ray, S.; Okamoto, K; Okamoto, M. *Macromolecules* **2003**, *36*, 2719.
(25) Chang, J. H.; An, Y; Sur, G. S. *J. Polym. Sci., Part B: Polym. Phys.* **2003**, *41*, 94.
(26) Ray, S. S.; Yamada, K.; Okamoto, M; Ueda, K. *Nano Lett.* **2002**, *2*, 1093–1096.
(27) Krikorian, V.; Pochan, D. J. *Chem. Mater.* **2003**, *15*, 4317–4324.
(28) Krikorian, V.; Pochan, D. *Macromolecules* **2004**, *37*, 1680–1691.
(29) Krikorian, V.; Pochan, D. *Macromolecules* **2005**, *38*, 6520–6527.
(30) Wu, L.; Hou, H. *J. Appl. Polym. Sci.* **2010**, *115*, 702.
(31) Moon, S.-I.; Lee, C. W.; Taniguchi, I.; Miyamoto, M.; Kimura, Y. *Polymer* **2001**, *42*, 5059.
(32) Mano, J. F.; Wang, Y. M.; Viana, J. C.; Denchev, Z.; Oliveira, M. *J. Macromol. Mater. Eng.* **2004**, *289*, 910.
(33) Yaman, M.; Ozkaya, S; Vasanthan, N. *J. Polym. Sci., Part B: Polym. Phys.* **2008**, *46*, 1497.
(34) Ogata, N.; Jimenez, G.; Kawai, H.; Ogihara, T. *J. Polym. Sci., Part B: Polym. Phys.* **1997**, *35*, 389.
(35) Fischer, E. W.; Sterzel, H. J.; Wegner, G. *Kolloid Z. Z. Polym.* **1973**, *251*, 980.
(36) Via, R. A.; Liu, W. *J. Polym. Sci., Part B: Polym. Phys.* **2002**, *40*, 1590.
(37) Krikorian, V.; Kurian, M.; Galvin, M. E.; Noewak, A. P.; Deming, T. J.; Pochan, D. J *J. Polym. Sci., Part B: Polym. Phys.* **2002**, *40*, 2579.
(38) Maiti, P.; Batt, C. A.; Giannelis, E. P. *Biomacromolecules* **2007**, *8*, 3393.
(39) Giannelis, E. P. *Adv. Mater.* **1996**, *8*, 29.
(40) Lincoln, D. M.; Vaia, R. A.; Krishnamoorti, R. *Macromolecules* **2004**, *37*, 4554.
(41) Avrami, M. *J. Chem. Phys.* **1939**, *7*, 1103.
(42) Avrami, M. *J. Chem. Phys.* **1941**, *9*, 177.

(43) Zhang, J.; Tsuji, H.; Noda, I.; Ozaki, Y. *Macromolecules* **2007**, *37*, 6433–6439.
(44) Zhang, J.; Duan, Y.; Sato, H.; Tsuji, H.; Noda, I.; Yan, S.; Ozaki, Y. *Macromolecules* **2005**, *38*, 8012.
(45) Kister, G.; Cassanas, G.; Vert, M. *Polymer* **1998**, *39*, 267.
(46) Ikada, Y.; Jamishidi, K.; Tsuji, H.; Hyon, S.-H. *Macromolecules* **1987**, *20*, 904.
(47) Kalb, B.; Pennings, A. J. *Polymer* **1980**, *21*, 607.
(48) DeSantis, P.; Kovacs, A. J. *Biopolymers* **1968**, *6*, 299.
(49) Hoogsteen, W.; Postema, A. R.; Penning, A. J.; ten Brinke, G.; Zugenmaiier, P. *Macromolecules* **1990**, *23*, 634–642.
(50) Vasanthan, N; Ly, O. *Polym. Degrad. Stab.* **2009**, *94*, 1364.